Available online at www.sciencedirect.com

ScienceDirect

Procedia Structural Integrity 13 (2018) 813–818

Structural Integrity Procedia

www.elsevier.com/locate/procedia

ECF22 - Loading and Environmental effects on Structural Integrity

A discussion about multi-axial fatigue criteria for NiTinol cardiovascular devices

Francesca Berti[a], Lorenza Petrini[b]*, Andrea Spagnoli[c]

[a] *Department of Chemistry, Materials and Chemical Engineering "Giulio Natta", Politecnico di Milano, 20133 Milano (Italy)*
[b] *Department of Civil and Environmental Engineering, Politecnico di Milano, Piazza Leonardo da Vinci 32, 20133 Milano (Italy)*
[c] *Department of Engineering and Architecture, Università di Parma, Parco Area delle Scienze, 181/A - 43124 Parma (Italy)*

Abstract

Nickel-Titanium (NiTinol) alloys exploit a typical super-elastic behavior which makes them suitable for many biomedical applications, among which peripheral stenting, requiring the device being subjected to the high mobility of the lower limbs. Unfortunately, this complex environment can lead to the device fatigue fracture with likely other more severe complications, e.g. restenosis. Standards require to experimentally verify stent fatigue life behavior, without giving indications on how to select the loads to be applied for resembling most critical in-vivo conditions. Moreover, different multi-axial fatigue criteria have been originally developed for standard metals to predict the behavior under cyclic loads, but none of them is specifically formulated for NiTinol. This paper presents a numerical study having two aims: i) understanding how non-proportional loading conditions due to combination of axial compression, bending and torsion induced at each patient gait on the femoro-popliteal artery affects the implanted stent stress/strain distribution; ii) understanding how stent fatigue life prediction may be affected by the choice of the fatigue criteria. Accordingly, two different peripheral stent geometries, resembling commercial ones, were analysed under different sets of loading conditions. The cyclic deformations induced over the device structure by macroscopic loads are interpreted through four different fatigue approaches recently used in Nitinol fatigue analyses: Von Mises, Fatemi-Socie, Brown-Miller and Smith-Watson-Topper. The comparison between the outputs highlights that they are strongly influenced by the loading path, recognizing the major role in fatigue due to the combined torsional and bending actions. On the other hand, the choice of the fatigue criterion impacts on the fatigue life prediction.

© 2018 The Authors. Published by Elsevier B.V.
Peer-review under responsibility of the ECF22 organizers.

Keywords: shape memory alloys; multi-axial fatigue; NiTinol; peripheral stents

E_M	elastic modulus for the austenite phase	k, S	empirical material constant accounting for the coupling of shear/bending fatigue limit

* Corresponding author. Tel.: +39 02 2399 4307; fax: +39 02 2399 4286.
E-mail address: lorenza.petrini@polimi.it

2452-3216 © 2018 The Authors. Published by Elsevier B.V.
Peer-review under responsibility of the ECF22 organizers.
10.1016/j.prostr.2018.12.156

E_A	elastic modulus for the austenite phase	σ_y	material monotonic yield strength
ε_a^{VM}	alternate equivalent strain	σ_{max}	maximum normal stress
ε_a	alternate normal strain	$\sigma_{n,max}$	maximum normal stress on the critical plane
ε_L	maximum residual strain	σ_{SSA}	starting stress value for the reverse phase transformation
$\frac{\Delta\varepsilon_1}{2}$	first principal component of the alternate strain tensor	σ_{SAS}	starting stress value for the forward phase transformation
$\frac{\Delta\varepsilon_2}{2}$	second principal component of the alternate strain tensor	σ_{FSA}	final stress value for the reverse phase transformation
$\frac{\Delta\varepsilon_3}{2}$	third principal component of the alternate strain tensor	σ_{FAS}	final stress value for the forward phase transformation
$\frac{\Delta\varepsilon_n}{2}$	normal strain amplitude on the critical plane of maximum shear strain	σ_{SAS}^C	tarting stress value for the forward phase transformation in compression
$\frac{\Delta\gamma_{max}}{2}$	maximum shear strain amplitude on the critical plane of maximum shear strain	σ_{SAS}^C	tarting stress value for the forward phase transformation in compression
$\frac{\Delta\varepsilon_{max}}{2}$	maximum normal strain amplitude on the plane of maximum normal strain		

1. Introduction

Peripheral occlusive pathologies are caused in more than 90% of the cases by atherosclerosis, which can lead to a broad spectrum of severe consequencies (Cimminiello, 2002). One recognized cause for the high incidence of peripheral occlusions is the wide mobility of the legs leading the femoro-popliteal artery (FPA) to highly deform under axial, torsional and bending actions (Ansari *et al.*, 2013; MacTaggart *et al.*, 2014). Many efforts have been spent trying to quantify the amount of these multi-axial loads (Cheng *et al.*, 2006; Klein *et al.*, 2009). The clinical scenario changes when a stent is implanted, introducing a local stiffening and influencing the macroscopic deformations (Gökgöl *et al.*, 2016). Endovascular stenting is actually recognized as the clinical gold standard for the revascularization. At the peripheral level it is performed using NiTinol stents: their super-elastic behavior allows the withstanding of serios deformations without experiencing permanent shape change and the long-term results are promising (Schillinger *et al.*, 2006). However, the cyclic loads experienced during gait can be responsible of the fatigue failure of the device (Petrini *et al.*, 2016) with possible drawbacks such as in-stent restenosis (Scheinert *et al.*, 2005; Gökgöl *et al.*, 2016). No specific indications are given by international agencies or standards about NiTinol fatigue life prediction, but it is recognized that finite element analysis (FEA) can be a useful tool to have a better insight of the cyclic state of stress and strain acting on the device under physiological conditions. Since experimental campaigns are expensive both in terms of cost and time, the best approach is based on minimizing the experiments to the worst case scenario only, using FE tools to examine many other possible in-vivo clinical conditions.

Hence, the results of the FEA need to be interpreted through fatigue approaches to assess the risk of failure. In literature many criteria have been proposed for metals, either in case of applied proportional or non-proportional loads, but none is specifically indicated for NiTinol and no previous knowledge is able to assess whether they are all equivalent. The aim of this work is to numerically investigate the in-vivo boundary conditions acting on the stented FPA, assessing which combination represents the worst scenario in terms of the device fatigue failure. Then, different fatigue approaches are examined to find out if an agreement in the prediction exists.

Since gate provokes movements of muscles that affect in different way the FPA deformation, it is likely that the loading components are non-proportionally applied. Moreover, even in case of a proportional macroscopic load, it is not sure that the proportionality is guaranteed at the stent local level for the aforementioned reasons. In this way, the standard Von Mises approach seems not to be adequated for a reliable interpretation (Auricchio *et al.*, 2016). Other multi-axial fatigue criteria, namely the Fatemi-Socie, the Brown-Miller and Smith-Watson-Topper, are considered: they are based on the concept of the critical plane, which is the location of the maximum stress responsible for crack initiation in a polar coordinate system (Pelton *et al.*, 2013; Mahtabi, Shamsaei and Rutherford, 2015).

2. Materials and methods

The FE validated models of two different stents, namely stent A and C resembling commercial ones (Figure 1), were available from the previous work of Allegretti et al. (2008): we refer to this paper for the knowledge of all the FE model details. A multi-modal simulation is implemented into the FE solver Abaqus Standard 2017 (Dassault Sistémes, SIMULIA, Providence, RI) using the same devices. The NiTInol material properties, considered equal for both the geometries, are described through the ABQ_SUPER_ELASTIC material model, available in the solver. The used material parameters are: E_A=47000 MPa, E_M= 22000 MPa, ν= 0.3, ε_L= 0.045, σ_{SAS}= 260 MPa, σ_{FAS}= 350 MPa, σ_{SSA}= 140 MPa, σ_{FSA}= 80 MPa, σ_{SAS}= 516 MPa. All the simulation steps are conducted at a fixed temperature of 37 °C to reproduce the in-vivo environment.

The first preload phase is computed to mimic the stent crimping and implantation, introducing a value of mean strain at each location of the structure from which the fatigue load pulses. The mean strain distribution changes point to point in the stent, but it does not overcome the 3%:this guarantee initial conditions compatible with the post-implantation scenario in terms of internal strains

The amount of axial compression, torsional and bending actions during the fatigue cycle are chosen according to literature physiological data (Ansari *et al.*, 2013; MacTaggart *et al.*, 2014). In particular, the maximum axial excursion is about 4%, while a 6°/cm torsion and a 20 mm radius of curvature bending are choosen. Different loads combinations are examined, considering both in-phase and counterphase loads (Table 1): the nominal fatigue ratio of the applied displacements/rotations is R=0. However, since the cyclic loads are applied starting from conditions reached after crimping and deployment, the effective fatigue ratio could be different.

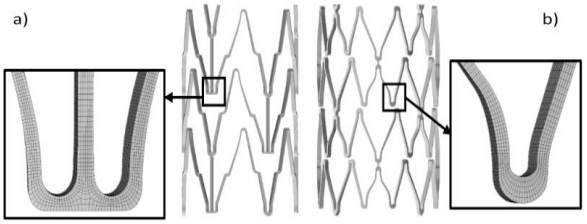

Figure 1 Stent A model and details of the mesh (a) and Stent C model and details of the mesh (b).

Table 1 Different loading conditions applied during the numerical analysis. Both proportional (P) and non-proportional (NP) loading conditions are explored. Caso 0: in-phase axial compression (A), bending (B) and torsional (T) actions. Three different combinations are created for each of the three NP cases. The C apex, when present, indicates that the load is maintained constant throughout the cycle at the value reached at the end of crimping and deployment. . The I apex, when present, indicates that the load is applied counterphase, namely its peak is reached at the valley of the other loads.

Case 0 (P)		A, B, T	
Case 1 (NP)	A, B^C, T^C	A^C, B, T^C	A^C, B^C, T
Case 2 (NP)	A, B, T^C	A^C, B, T	A, B^C, T
Case 3 (NP)	A, B^I, T	A^I, B, T	A, B, T^I

The four fatigue approaches considered in this study are based on a different definition of the quantity measuring the fatigue index. The von Mises (VM) criterion chooses as fatigue index the equivalent alternate strain (Eq. 1). The the Fatemi-Socie (FS) is a strain-based critical plane model for shear failure mode materials and recognizes as the fatigue index a function of the maximum amplitude of shear strain and the maximum value of normal stress calculated on the maximum shear strain plane (Eq. 2). The Brown-Miller (BM) is also a strain-based approach and the fatigue index is defined as an equivalent amplitude shear strain, given by combination of the maximum shear strain amplitude and normal strain amplitude that occurs in a cycle on the maximum shear strain plane (Eq. 3). The Smith-Watson-Topper (SWT) is an energy-based approach and the fatigue index is given by the product of the maximum normal stress and the maximum normal strain amplitude, both on the plane of maximum normal strain (Eq. 4).

$$VM = \frac{1}{2(1+\nu)\sqrt{2}}\sqrt{(\Delta\varepsilon_1 - \Delta\varepsilon_2)^2 + (\Delta\varepsilon_2 - \Delta\varepsilon_3)^2 + (\Delta\varepsilon_3 - \Delta\varepsilon_1)^2} \quad (1)$$

$$FS = \frac{\Delta\gamma_{max}}{2}\left(1 + k\frac{\sigma_{n,max}}{\sigma_y}\right) \quad (2)$$

$$BM = \frac{\Delta\gamma_{max}}{2} + S\frac{\Delta\varepsilon_n}{2} \quad (3)$$

$$SWT = \sigma_{n,max}\ \frac{\Delta\varepsilon_{max}}{2} \quad (4)$$

For each of the considered loading conditions, the stress and strain tensors at the fatigue peak and valley are extracted from the centroid of each finite element of the stent numerical models and processed through an ad-hoc MATLAB code (MathWorks). The value of the fatigue index according to the four criteria above at every location for each model is plotted against the corresponding first principal mean strain. Each cloud of points is compared with a material limit curve, specifically built for each criterion, which was previously assessed through cyclic axial tensile tests performed on dogbone samples, as detailed in Allegretti et al. (Allegretti *et al.*, 2018). A fatigue risk factor, defined as the normalized distance between the points and the limit curve, is calculated for each case. A value for the risk factor greater than 1 means a critical condition in which fatigue failure is expected before 10^6 cycles.

3. Results

For each stent under the same loading condition, the choice of a specific multi-axial fatigue criterion strongly influences the prediction. From the load case 0 is it immediately clear how the approaches give different interpretation of the internal state of the devices. In particular, the VM tends to overestimate the fatigue risk compared to the other criteria, showing many points overcoming the limit curve (Figure 2a and 2b) and a higher risk factor with respect to other approaches, the stent being equal (Figure 2c left). However, all the criteria are indicating the same most critical area. The stent geometry is a factor which affect the macroscopic response, so the clouds morphology: stent A is characterized by a more compliant structure than stent C (Allegretti *et al.*, 2018). This is confirmed by the fatigue plots: stent A has a fewer number of elements subjected to high deformations since the structure itself accommodates for the major part of the macroscopic load. On the other hand, the stiffer stent C transmits an higher deformation to the whole structure, resulting in a major number of elements subjected to high loads. Accordingly, the risk factor considering the same criterion (Figure 2c right) is higher for stent C (2.03) than for stent A (1.96).

As expected, by switching to the other load cases (NP) the cloud of points and the risk factor change accordingly. For simplicity, only the results regarding stent A are summarized in this section. From the load case 1, where only one load components is cycled, it is easy to address the major causes for fatigue fracture to the bending and torsional ones Figs. 3b-3c, respectively. In particular, under cyclic bending load all the criteria show a cloud of points at least close to the limit curve, with VM (1.69) and FS (1.33) predicting failure. When the cyclic load is purely axial, Fig. 3a, all the criteria agree in computing a risk factor far below the unit. As expected, load case 2 highlights how the combination of bending and torsional loads lead to high risk factors, specifically 3.1 for VM, 1.85 for FS, 1.57 for BM and 1.64 for SWT, Fig. 3e. For the other combinations, only the VM predicts a risk of failure (Figure 3d and 3f), even if very low (1.07 and 1.01 respectively). Also for NP loads the same critical area is identified by all the criteria. At last, the load case 3 suggests how the presence of a counterphase axial load increase dramatically the level of criticality for the stent endurance, Fig. 4.

4. Discussions and conclusions

This study performed a numerical analysis aimed at inspecting different multi-axial loads combinations, mimicking the FPA environment. Four different fatigue criteria were implemented to give an interpretation of the severity of the conditions according to different indices. VM criterion indicates high risk factors in the majority of the cases. FS, BM and SWT predictions are more influenced by the loads combination and their predictions usually agree, even if their fatigue indices are based on different mechanical quantities. All the approaches recognize the same most critical area for fracture in all the combinations. This is motivated by the geometrical characteristics of the stent, resulting in more weak areas especially in the double V-strut of the stent A and the simple strut of stent C. Moreover, all of them agrees in stating that the axial load in counterphase (second combination of case 3) is the most dangerous one.

Despite the encouraging results toward a better understanding of the fatigue behavior, some limitations need to be accounted: FS and BM indices are dependent on material empirical constants herein taken as 1(Socie, Waill and Dittmer, 1985; Shamsaei and Fatemi, 2009). A preliminary sensitivity analysis has been performed showing how the prediction can slightly vary by changing their value. The structural limit curve was derived from axial fatigue tests on dogbone samples, since other multi-axial components would have been impossible to test with such material specimens. More tests should be addressed to the more accurate characterization of the limit curve. This is a numerical only study from which we can conclude that the VM gives a different interpretation compared to the critical plane approaches. Some experimental tests are mandatory to finally conclude which fatigue criterion is the most accurate treating NiTinol devices

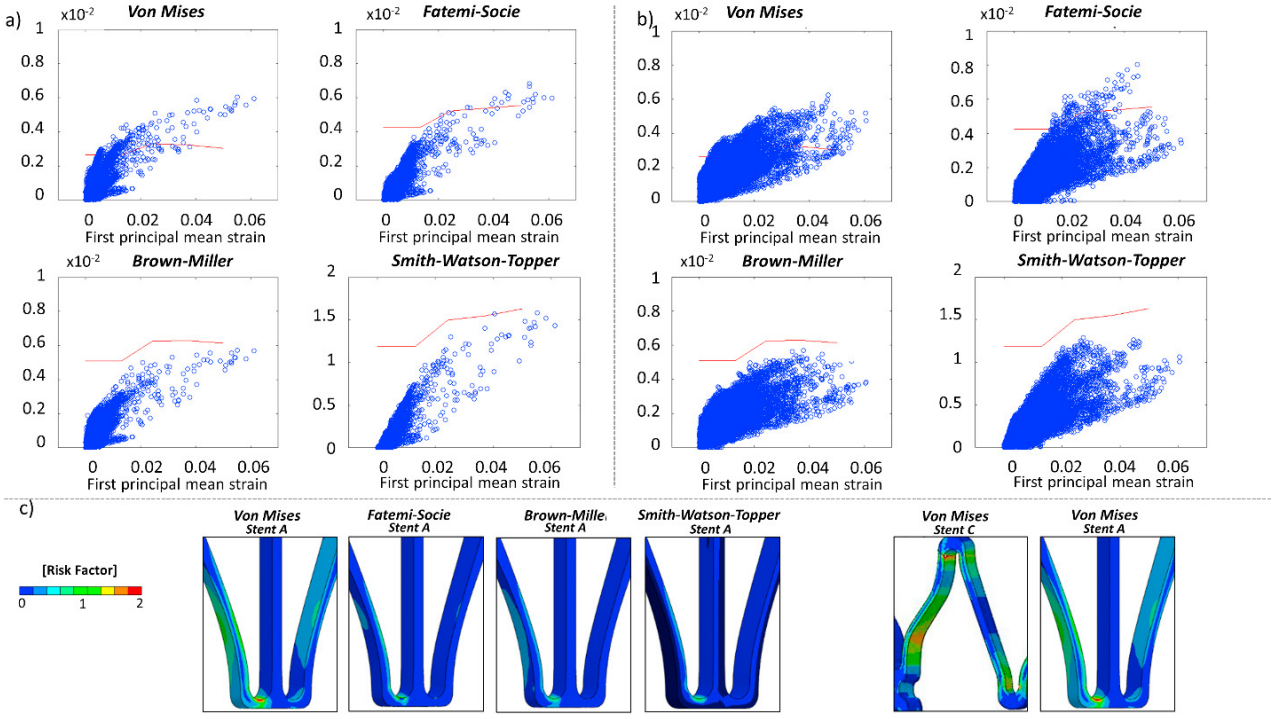

Figure 2 Results of the load case 0 (P) for stent A (a) and C (b). The clouds of points are representative of the output of each criterion at every centroid of the stent mesh. Points overcoming the fatigue limit curve for 10^6 cycles (red line) are considered critical for fatigue failure. Risk factor color maps (c): comparison among all the criteria for stent A (left) and between the two stents for the Von Mises criterion (right).

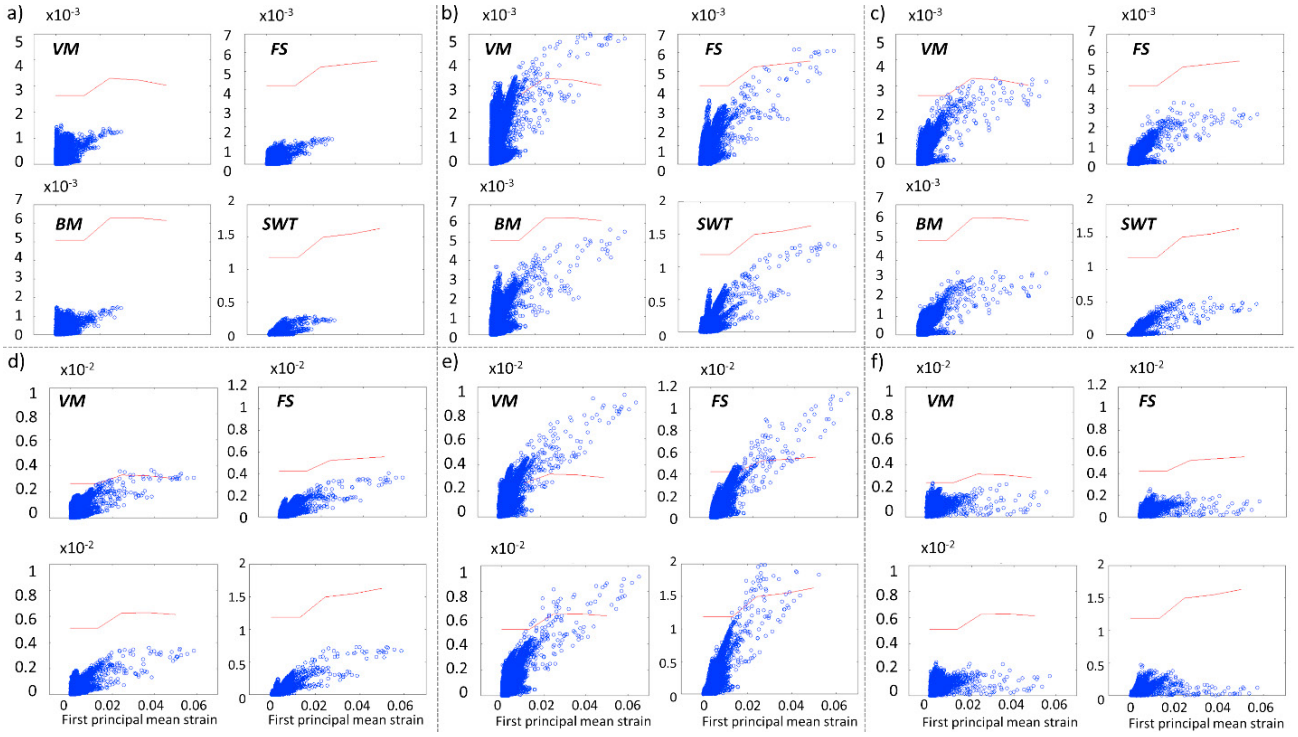

Figure 3 Results of the load case 1 and 2 (NP) for stent A under different loading combinations. (a) constant bending and torsion, cyclic axial compression, (b) constant axial and torsion, cyclic bending, (c) constant axial and bending, cyclic torsion, (d) constant torsion, cyclic axial and bending, (e) constant axial, cyclic bending and torsion, (f) constant bending, cyclic axial and torsion.

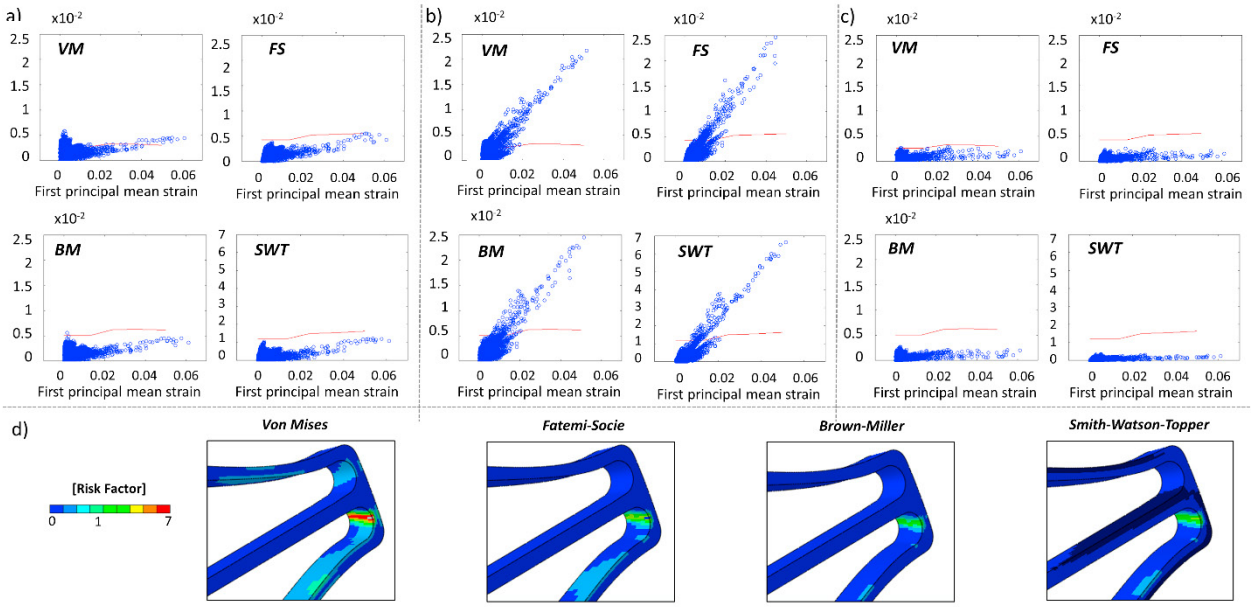

Figure 4 Results of the load case 3 (NP) for stent A under different loading combinations. (a) cyclic axial and torsion, alternating bending, (b) cyclic bending and torsion, alternating axial, (c) cyclic axial and bending, alternating torsion. Risk factor color maps (d) are given for the case showed in (b)

References

Allegretti, D. *et al.* (2018) 'Fatigue Assessment of Nickel–Titanium Peripheral Stents: Comparison of Multi-Axial Fatigue Models', *Shape Memory and Superelasticity*. Springer International Publishing, 4(1), pp. 186–196. doi: 10.1007/s40830-018-0150-7.

Ansari, F. *et al.* (2013) 'Design considerations for studies of the biomechanical environment of the femoropopliteal arteries', *Journal of Vascular Surgery*. Elsevier Inc., 58(3), pp. 804–813. doi: 10.1016/j.jvs.2013.03.052.

Auricchio, F. *et al.* (2016) 'A shakedown analysis of high cycle fatigue of shape memory alloys', *International Journal of Fatigue*. Elsevier Ltd, 87, pp. 112–123. doi: 10.1016/j.ijfatigue.2016.01.017.

Cheng, C. P. *et al.* (2006) 'In Vivo MR Angiographic Quantification of Axial and Twisting Deformations of the Superficial Femoral Artery Resulting from Maximum Hip and Knee Flexion', *Journal of Vascular and Interventional Radiology*, 17(6), pp. 979–987. doi: 10.1097/01.RVI.0000220367.62137.E8.

Cimminiello, C. (2002) 'PAD - Epidemiology and pathophysiology', *Thrombosis Research*, 106(6). doi: 10.1016/S0049-3848(01)00400-5.

Gökgöl, C. *et al.* (2016) 'In-Vivo Quantification of Femoro-popliteal Artery Deformations: Percutaneous Transluminal Angioplasty vs. Nitinol Stent Placement', *Journal of Endovascular Therapy*.

Klein, A. J. *et al.* (2009) 'Quantitative assessment of the conformational change in the femoropopliteal artery with leg movement', *Catheterization and Cardiovascular Interventions*, 74(5), pp. 787–798. doi: 10.1002/ccd.22124.

MacTaggart, J. N. *et al.* (2014) 'Three-dimensional bending, torsion and axial compression of the femoropopliteal artery during limb flexion', *Journal of Biomechanics*. Elsevier, 47(10), pp. 2249–2256. doi: 10.1016/j.jbiomech.2014.04.053.

Mahtabi, M. J., Shamsaei, N. and Rutherford, B. (2015) 'Mean strain effects on the fatigue behavior of superelastic Nitinol alloys : An experimental investigation', in *Procedia Engineering*. Elsevier B.V., pp. 646–654. doi: 10.1016/j.proeng.2015.12.645.

Pelton, A. R. *et al.* (2013) 'Rotary-bending fatigue characteristics of medical-grade Nitinol wire', *Journal of the Mechanical Behavior of Biomedical Materials*, 27, pp. 19–32.

Petrini, L. *et al.* (2016) 'A Computational Approach for the Prediction of Fatigue Behaviour in Peripheral Stents: Application to a Clinical Case', *Annals of Biomedical Engineering*, 44(2), pp. 536–547. doi: 10.1007/s10439-015-1472-7.

Scheinert, D. *et al.* (2005) 'Prevalence and clinical impact of stent fractures after femoropopliteal stenting', *Journal of the American College of Cardiology*. Elsevier Masson SAS, 45(2), pp. 312–315. doi: 10.1016/j.jacc.2004.11.026.

Schillinger, M. *et al.* (2006) 'Balloon Angioplasty versus Implantation of Nitinol Stents in the Superficial Femoral Artery', *New England Journal of Medicine*, 354.

Shamsaei, N. and Fatemi, A. (2009) 'Effect of hardness on multiaxial fatigue behaviour and some simple approximations for steels', *Fatigue and Fracture of Engineering Materials and Structures*, 32(8), pp. 631–646. doi: 10.1111/j.1460-2695.2009.01369.x.

Socie, D. F., Waill, L. A. and Dittmer, D. F. (1985) 'Biaxial fatigue of Inconel 718 including mean stress effects', *Multiaxial Fatigue*, pp. 463–481. doi: https://doi.org/10.1520/STP36238S.